

Constraining the Higgs couplings to up and down quarks using production kinematics at the CERN Large Hadron Collider

Gage Bonner and Heather E. Logan*

*Ottawa-Carleton Institute for Physics, Carleton University,
1125 Colonel By Drive, Ottawa, Ontario K1S 5B6, Canada*

(Dated: August 15, 2016)

We study the prospects for constraining the Higgs boson's couplings to up and down quarks using kinematic distributions in Higgs production at the CERN Large Hadron Collider. We find that the Higgs p_T distribution can be used to constrain these couplings with precision competitive to other proposed techniques. With 3000 fb^{-1} of data at 13 TeV in the four-lepton decay channel, we find $-0.73 \lesssim \bar{\kappa}_u \lesssim 0.33$ and $-0.88 \lesssim \bar{\kappa}_d \lesssim 0.32$, where $\bar{\kappa}_q = (m_q/m_b)\kappa_q$ is a scaling factor that modifies the q quark Yukawa coupling relative to the Standard Model bottom quark Yukawa coupling. The sensitivity may be improved by including additional Higgs decay channels.

I. INTRODUCTION

If the Standard Model (SM) of particle physics is to be complete, then there must be a mechanism through which elementary particles acquire mass. The Higgs mechanism achieves this purpose, and a particle with the required properties was recently observed by the ATLAS and CMS collaborations at the CERN Large Hadron Collider (LHC) [1, 2]. We can test some of the predictions of the SM by studying the Higgs boson's couplings to other particles. The SM does not numerically predict these couplings directly; it postulates relatively simple expressions for their size in terms of other observables. Therefore, if we can measure these observables (particle masses, mixing angles, etc.) while characterizing the strength of the Higgs couplings via its production and decay rates, we can determine whether or not the relations predicted by the SM are correct. This gives us a clue as to whether or not the SM Higgs mechanism actually provides masses for all constituents of the SM.

For heavy gauge bosons W and Z we expect the Higgs couplings to be equal to $2m_{W,Z}^2/v$ in the SM, where $v \approx 246 \text{ GeV}$ is the Higgs vacuum expectation value. The measured couplings have been found to be consistent with the SM within experimental error [3, 4]. In the fermion sector, we expect the Higgs couplings to quarks q to be equal to m_q/v in the SM. This is also true for charged leptons. The quantities m_q/v are usually called the Yukawa couplings y_q . Since the couplings are proportional to the quark masses, we expect Higgs-mediated processes to be dominated by the heavy (top and bottom) quark contributions. Indeed, Higgs production is controlled mainly by gluon fusion whereby two gluons initiate a heavy quark loop which ejects a Higgs boson. There are several experimental analyses which probe the Higgs couplings to the heavy (top and bottom) quarks [5–12]. These are also found to be consistent within uncertainties with the SM prediction, so we conclude that the SM Higgs mechanism is a valid theory for the origin of

the heavy gauge bosons' and quarks' masses.

The situation is less clear for lighter quarks. Constraining the light quark Yukawa couplings is important since there are alternate models in which they differ from the SM expectation [13–16] or do not enter at all [17]. Constraints can be placed on the charm and strange quark Yukawa couplings using inclusive Higgs production rates in various SM decay channels [18–21] and through exclusive radiative mesonic decays, $h \rightarrow V\gamma$, where V is a charmonium or $s\bar{s}$ meson [22–24] (see also Refs. [19, 21]). The charm Yukawa coupling is expected to be measured at a future International Linear e^+e^- Collider to high precision using the anticipated excellent charm tagging in the low-background e^+e^- collision environment [25].

Up and down quark Yukawa couplings are by far the hardest to constrain: at the LHC it is basically impossible to distinguish Higgs decays to up and down quark jets from $h \rightarrow gg$ or $h \rightarrow s\bar{s}$.¹ Furthermore, since the cross section for quark fusion, $q\bar{q} \rightarrow h$, is proportional to the square of the relevant quark Yukawa coupling y_q^2 , for SM couplings proton collisions are much more likely to result in $b\bar{b} \rightarrow h$ than $u\bar{u} \rightarrow h$ and $d\bar{d} \rightarrow h$ even though u, d are the valence quarks of the proton. In particular, the up and down quark masses are $m_u = 2.3_{-0.5}^{+0.7} \text{ MeV}$ and $m_d = 4.8_{-0.3}^{+0.5} \text{ MeV}$ ($\overline{\text{MS}}$ masses evaluated at $\mu \simeq 2 \text{ GeV}$) while $m_b = 4.18 \pm 0.03 \text{ GeV}$ ($\overline{\text{MS}}$ mass evaluated at m_b) [27].

It is customary to parametrize the deviations of the Yukawa couplings from their SM values using scaling factors κ_q [28], so that the coupling terms in the Lagrangian become $-\kappa_q y_q^{\text{SM}} \bar{q}qh$, with $\kappa_q = 1$ corresponding to the SM. We will adopt the convention of Ref. [23] in which the light quark couplings are all scaled relative to the bottom quark coupling. This greatly reduces the theoretical uncertainty in the reference coupling since the bottom quark mass has a much smaller experimental uncertainty than the up and down quark masses. It also facilitates comparisons with the literature. Since the Yukawa cou-

* logan@physics.carleton.ca

¹ On the other hand, Ref. [26] showed that a statistical discrimination between gluon jets and light-quark jets is possible using jet energy profiles.

plings are proportional to the relevant quark mass, we have

$$\bar{\kappa}_q = \frac{m_q}{m_b} \kappa_q, \quad (1)$$

where $\bar{\kappa}_q$ is the light quark coupling scaled relative to that of the bottom quark. In the SM we expect $\bar{\kappa}_u \simeq 4.7 \times 10^{-4}$ and $\bar{\kappa}_d \simeq 1.0 \times 10^{-3}$ [23].

The current tightest constraints on up and down quark Yukawa couplings come from Higgs production and decay rates. A global fit to all on-resonance Higgs data, allowing all of the Higgs couplings to vary, yields $|\bar{\kappa}_u| < 1.3$ and $|\bar{\kappa}_d| < 1.4$ at 95% confidence level [23]. Fixing all Higgs couplings to their SM values except for one of the up or down quark Yukawa couplings at a time instead yields $|\bar{\kappa}_u| < 0.98$, $|\bar{\kappa}_d| < 0.93$, again at 95% confidence level [23]. An alternative method [29] considers the inclusive $pp \rightarrow h \rightarrow 4\ell$ production rate in the off-shell region, which is unaffected by the total Higgs width; current data yields limits less sensitive by about a factor of two than the on-shell fits.

Two completely different methods for constraining the up and down Yukawa couplings have recently been proposed. The first relies on measuring isotope shifts in atomic clock transitions, which can be affected by Higgs exchange as well as the usual electroweak gauge boson exchange [30]. This method depends strongly on the precision of future isotope shift measurements and on an accurate theoretical determination of the electroweak gauge contribution; nevertheless, it may yield constraints at a level comparable to the Higgs coupling fit described above. The second relies on a future discovery of Higgs-portal dark matter; in such a scenario, if the dark matter relic density is set by the usual thermal freeze-out, current direct-detection limits already constrain the light quark Yukawa couplings at the level of $|\bar{\kappa}_{u,d}| \lesssim 0.01$ [31].

In this paper we propose a complementary technique to constrain the Higgs couplings to up and down quarks using the Higgs boson production kinematics at the LHC. If the shapes of the Higgs kinematic distributions from gluon-fusion production are sufficiently different from the shapes of the same distributions initiated by quark fusion, a measurement of these distributions can be used to discriminate between them and set limits on the fraction of Higgs events produced via quark fusion. There are good theoretical reasons to expect the kinematic distributions for Higgs production via $u\bar{u}$ or $d\bar{d}$ fusion to be different from those via gluon fusion. The Higgs transverse momentum (p_T) distribution is shaped mainly by the additional jet radiation from the initial-state partons, which is controlled by the strong charges and spins of the initial-state partons. Indeed, we find that the gluon-fusion process has a harder p_T distribution than quark fusion, allowing these to be discriminated. For concreteness, we parametrize the Higgs p_T distributions in terms of a high- p_T /low- p_T asymmetry parameter and determine the optimum division between the high- and low- p_T regions.

We would also expect the Higgs longitudinal momentum (p_z) to be smaller (more central) in the gluon-fusion process and larger in the quark-fusion processes, due to the asymmetry in the average proton momentum fraction carried by a valence quark and the corresponding antiquark. However, after taking into account the detector acceptance for the Higgs decay products in the four-lepton channel, we find that the p_z distributions do not provide additional sensitivity. This distribution may be worthy of further study in the diphoton decay channel.

This paper is organized as follows. In Section II we derive the condition on the gluon and up- and down-quark couplings which ensures that the total rate in the 4 lepton channel is the same as in the SM. This makes our method statistically independent from the fit to signal strengths. We then compute the cross sections, branching ratios and detection efficiencies that we will need for all the relevant processes using MadGraph5_aMC@NLO [32]. Section III defines the asymmetry observable of our method and provides sample momentum distributions from simulations. We determine the expected statistical uncertainty on the up and down quark Yukawa couplings with 300 and 3000 fb⁻¹ of integrated luminosity at the 13 TeV LHC. Section IV gives some context for the strength of our constraints and summarizes our conclusions. Appendix A contains a derivation of the statistical error on our asymmetry observable.

II. HIGGS PRODUCTION CROSS SECTIONS

We consider $pp \rightarrow h \rightarrow 4\ell$, with $\ell = e$ or μ . The background for the four-lepton final state is produced mainly by direct ZZ^* production via quark and gluon fusion [33]. The reason for using the 4ℓ final state is that this background is very small compared to the background in the diphoton channel, so that we can ignore it here. We also ignore Higgs production via vector boson fusion, associated production with a W or Z boson, and associated production with a $t\bar{t}$ pair; these processes can be separated out using other kinematic features. The observed rate for the signal process can then be written as

$$R(pp \rightarrow h \rightarrow 4\ell) = \sigma(pp \rightarrow h) \cdot \text{BR}(h \rightarrow 4\ell) \cdot \epsilon, \quad (2)$$

where $\sigma(pp \rightarrow h)$ is the total Higgs production cross section (including only our production modes of interest), $\text{BR}(h \rightarrow 4\ell)$ is the branching ratio of the Higgs to the four-lepton final state, and ϵ is the detector acceptance for this final state.

Our first task is to determine the relationship between $\bar{\kappa}_u$, $\bar{\kappa}_d$, and the hgg effective coupling κ_g (defined normalized to its SM value) that must be satisfied for the $pp \rightarrow h \rightarrow 4\ell$ rate to be equal to its SM expectation. We will assume that all other Higgs couplings besides these three are fixed to their SM values. In addition to computing the cross sections, including interference between the processes involving κ_g and $\bar{\kappa}_{u,d}$ that arises at next-to-leading order (NLO) in QCD, we must determine the

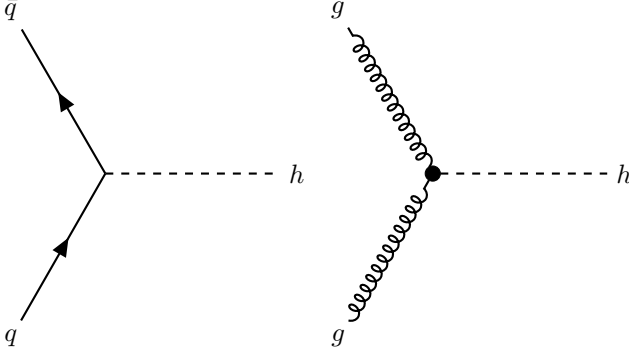


FIG. 1. The LO Feynman diagrams for Higgs production via quark fusion (left) and gluon fusion (right).

detector acceptances for the four leptons for each of these processes.

A. Production cross sections

Let us first consider the cross section $\sigma(pp \rightarrow h)$. At leading order (LO), the only two diagrams contributing to Higgs production are shown in Fig. 1. The Higgs boson is a color singlet, so it does not couple to gluons at tree level. However, one can introduce an effective vertex (shown in Fig. 1 as a black dot) which takes into account the fact that $gg \rightarrow h$ is mediated by a heavy quark loop; this is how gluon fusion Higgs production will be handled in our Monte Carlo simulations. The two diagrams in Fig. 1 have different particles in the initial state, so they do not interfere with each other at LO. We can then separate the gluon fusion and up- and down-quark fusion cross sections according to

$$\begin{aligned} \sigma^{\text{LO}}(pp \rightarrow h) &= \sigma_{gg}^{\text{LO}}(\kappa_g) + \sum_{q=u,d} \sigma_{q\bar{q}}^{\text{LO}}(\bar{\kappa}_q) \\ &= \kappa_g^2 \bar{\sigma}_{gg}^{\text{LO}} + \sum_{q=u,d} \bar{\kappa}_q^2 \bar{\sigma}_{q\bar{q}}^{\text{LO}}, \end{aligned} \quad (3)$$

where we define $\bar{\sigma}_{gg}^{\text{LO}}$ as the SM (i.e., $\kappa_g = 1$) gluon fusion Higgs production cross section computed at LO, and $\bar{\sigma}_{u\bar{u}}^{\text{LO}}$ and $\bar{\sigma}_{d\bar{d}}^{\text{LO}}$ as the appropriate quark fusion cross sections computed at LO with $\bar{\kappa}_{u,d} = 1$. Note that $\bar{\sigma}_{u\bar{u}}^{\text{LO}}$ and $\bar{\sigma}_{d\bar{d}}^{\text{LO}}$ are normalized in such a way that they are roughly six orders of magnitude larger than the corresponding SM cross sections.

At NLO the situation is more complicated. In addition to the virtual corrections, real radiation diagrams contribute, some of which give rise to interference as shown

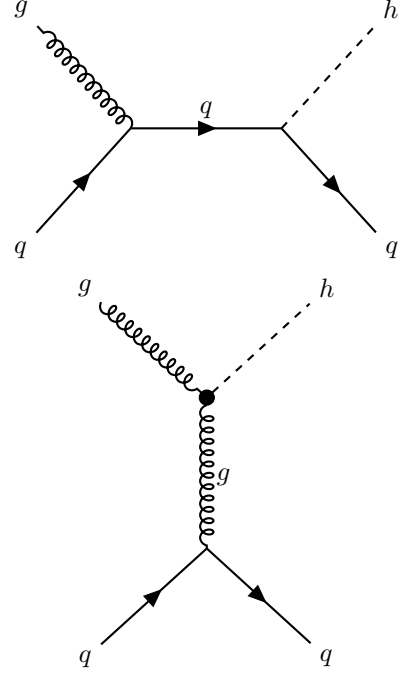


FIG. 2. Sample Feynman diagrams contributing to the real radiation part of the NLO cross section calculation. These diagrams involve the same initial- and final-state particles and hence contribute to the interference term.

in Fig. 2. We therefore have

$$\begin{aligned} \sigma^{\text{NLO}}(pp \rightarrow h) &= \sigma_{gg}^{\text{NLO}}(\kappa_g) + \sum_{q=u,d} \sigma_{q\bar{q}}^{\text{NLO}}(\bar{\kappa}_q) \\ &\quad + \sum_{q=u,d} \sigma_{q,\text{int}}^{\text{NLO}}(\kappa_g, \bar{\kappa}_q) \\ &= \kappa_g^2 \bar{\sigma}_{gg}^{\text{NLO}} + \sum_{q=u,d} \bar{\kappa}_q^2 \bar{\sigma}_{q\bar{q}}^{\text{NLO}} \\ &\quad + \sum_{q=u,d} \kappa_g \bar{\kappa}_q \bar{\sigma}_{q,\text{int}}^{\text{NLO}}, \end{aligned} \quad (4)$$

where we separate the gluon fusion, quark fusion, and interference pieces of the NLO cross section based upon their dependence on the coupling scaling factors κ_g , $\bar{\kappa}_u$, and $\bar{\kappa}_d$. The reference cross sections $\bar{\sigma}_{gg}^{\text{NLO}}$, $\bar{\sigma}_{q\bar{q}}^{\text{NLO}}$, and $\bar{\sigma}_{q,\text{int}}^{\text{NLO}}$ are defined with $\kappa_g = \bar{\kappa}_u = \bar{\kappa}_d = 1$.

In order to simulate Higgs events, we use MadGraph5_aMC@NLO 2.2.3 [32]. MadGraph automatically generates matrix elements for a process in terms of initial, final (and possibly intermediate) particles specified by the user. The default SM implementation in MadGraph explicitly sets the Yukawa couplings of the Higgs to up and down quarks equal to zero. Furthermore, one cannot easily generate $gg \rightarrow h$ since this coupling does not exist at tree level in the SM. In order to generate events which contain all the required Higgs interactions, we instead use the NLO Higgs Characterization model [34–37], which includes an effective vertex for the Higgs to gluon coupling

	LO	NLO
$\bar{\sigma}_{gg}$	16.55 ± 0.02 pb	37.3 ± 0.3 pb
$\bar{\sigma}_{u\bar{u}}$	13.44 ± 0.02 pb	15.4 ± 0.1 pb
$\bar{\sigma}_{d\bar{d}}$	9.48 ± 0.01 pb	11.2 ± 0.1 pb
$\bar{\sigma}_{u,\text{int}}$	–	14.5 ± 0.5 pb
$\bar{\sigma}_{d,\text{int}}$	–	10.6 ± 0.5 pb

TABLE I. Higgs production cross sections via gluon fusion, $u\bar{u}$ fusion, $d\bar{d}$ fusion, and interference, computed using MadGraph5_aMC@NLO 2.2.3 [32] for $\kappa_g = \bar{\kappa}_u = \bar{\kappa}_d = 1$ at LO and NLO in QCD.

as in Fig. 1. We introduce a further scaling factor κ_g to modify this vertex. We also modify the model by implementing Higgs couplings to up and down quarks, which we set equal to the Higgs coupling to bottom quarks with additional scaling factors $\bar{\kappa}_u$ and $\bar{\kappa}_d$. We use a Higgs mass of 125 GeV throughout.

We simulate Higgs events at the 13 TeV LHC at LO and NLO in QCD, with the NLO results matched to the parton shower. We use the NNPDF2.3.QED (LHAPDFID = 244600) parton distribution function sets [38] at the appropriate order in perturbation theory. We shower the events using Herwig++ 2.7.1 [39] and cluster the jets using the anti- k_T algorithm in FastJet 3.1.3 [40] (this last step is not strictly necessary for our analysis, since we will only consider the Higgs final-state momentum distributions in what follows). In this way we obtain the reference cross sections $\bar{\sigma}_{gg}^{\text{NLO}}$, $\bar{\sigma}_{q\bar{q}}^{\text{NLO}}$, and $\bar{\sigma}_{q,\text{int}}^{\text{NLO}}$ as in Eq. (4). The interference cross sections are obtained by defining a g, u, \bar{u} multiparticle, computing $(\bar{\sigma}_{gg} + \bar{\sigma}_{u\bar{u}} + \bar{\sigma}_{u,\text{int}})$, and then subtracting $\bar{\sigma}_{gg}$ and $\bar{\sigma}_{u\bar{u}}$ (and similarly for the down quark). Results are given in Table I. For comparison we have also computed the corresponding LO cross sections.² We do not decay the Higgs boson, so these cross sections are fully inclusive. The uncertainties quoted in Table I are the internal Monte Carlo integration uncertainties from MadGraph.

B. $h \rightarrow 4\ell$ branching ratio

Now let us consider the branching ratio $\text{BR}(h \rightarrow 4\ell)$. We would like to write this branching ratio in terms of κ_g , $\bar{\kappa}_u$ and $\bar{\kappa}_d$ as we have done with the cross section. Let Γ_{tot} be the total width of the Higgs boson. Then, by definition, we have

$$\text{BR}(h \rightarrow 4\ell) = \frac{\Gamma(h \rightarrow 4\ell)}{\Gamma_{\text{tot}}}. \quad (5)$$

² Note the large k -factor in going from LO to NLO for $\bar{\sigma}_{gg}$, and compare the state-of-the-art SM prediction $\bar{\sigma}_{gg} = 43.92$ pb from Ref. [41].

	LO	HXSWG
$\bar{\Gamma}_{gg}$	0.183 MeV	0.349 MeV
$\bar{\Gamma}_{u\bar{u}}$	4.34 MeV	2.35 MeV
$\bar{\Gamma}_{d\bar{d}}$	4.34 MeV	2.35 MeV
Γ_{else}	5.95 MeV	3.72 MeV
Γ_{ZZ^*}	0.090 MeV	0.107 MeV

TABLE II. Higgs partial widths for $\kappa_g = \bar{\kappa}_u = \bar{\kappa}_d = 1$. The first column shows the LO widths computed by MadGraph and the second shows the current state-of-the-art theoretical predictions from the LHC Higgs Cross Section Working Group (HXSWG) [41]. For the latter we take $\bar{\Gamma}_{u\bar{u}} = \bar{\Gamma}_{d\bar{d}} = \Gamma_{b\bar{b}}^{\text{SM}}$.

The coupling modification factors κ_g , $\bar{\kappa}_u$ and $\bar{\kappa}_d$ enter through their effect on the Higgs total width. In particular we have

$$\begin{aligned} \Gamma_{\text{tot}} &= \Gamma_{gg} + \sum_{q=u,d} \Gamma_{q\bar{q}} + \Gamma_{\text{else}} \\ &= \kappa_g^2 \bar{\Gamma}_{gg} + \sum_{q=u,d} \bar{\kappa}_q^2 \bar{\Gamma}_{q\bar{q}} + \Gamma_{\text{else}}, \end{aligned} \quad (6)$$

where $\bar{\Gamma}_{gg}$ is the SM (i.e., $\kappa_g = 1$) Higgs decay width to two gluons, $\bar{\Gamma}_{u\bar{u}}$ and $\bar{\Gamma}_{d\bar{d}}$ are the Higgs decay widths to $u\bar{u}$ and $d\bar{d}$ respectively with $\bar{\kappa}_u = \bar{\kappa}_d = 1$, and Γ_{else} is the Higgs partial width to all other SM final states, which we hold fixed to its SM value. The largest contribution to Γ_{else} comes from $h \rightarrow b\bar{b}$, followed by $h \rightarrow WW^*$. Because $\bar{\kappa}_q = 1$ implies that the q quark Yukawa coupling is set equal to the bottom quark Yukawa coupling, the partial width $\bar{\Gamma}_{q\bar{q}}$ is equal to the SM Higgs partial width to $b\bar{b}$ up to finite bottom quark mass effects, which are at the percent level and will henceforth be neglected. For these partial widths we will use the up-to-date SM theoretical predictions from the LHC Higgs Cross Section Working Group [41], which are reproduced in the last column of Table II. These include higher order QCD and electroweak corrections to Higgs decay partial widths, which can be quite sizable for Higgs decays to $q\bar{q}$.

C. Detector acceptance

Finally we need to determine the detector acceptances ϵ for each of the production processes. We compute these separately because we expect the different kinematic distributions of the different Higgs production processes to lead to different detector acceptances. We define an acceptance for each of the NLO reference cross sections in Eq. (4), and similarly for the LO reference cross sections.

To compute the acceptance for, e.g., the gluon fusion process, we generate the process $gg \rightarrow h \rightarrow 4\ell$ (including final states with electrons and/or muons), applying the

following kinematic cuts at the generator level:

$$\begin{aligned} p_{T,\ell} &> 10 \text{ GeV}, \\ |\eta_\ell| &< 2.5, \\ |m_{4\ell} - m_h| &< 1 \text{ GeV}, \end{aligned} \quad (7)$$

where $p_{T,\ell}$ is the transverse momentum and η_ℓ is the pseudorapidity of each of the four leptons, and $m_{4\ell}$ is the four-lepton invariant mass. The pseudorapidity cut approximates the angular acceptance of the inner trackers of the LHC detectors. The cut on the four-lepton invariant mass eliminates contributions from an off-shell Higgs boson, which can be significant when $m_{4\ell} > 2M_Z$. We then divide this decayed cross section by the corresponding reference cross section from Table I and by the branching ratio for $h \rightarrow 4\ell$. This yields the acceptance,

$$\epsilon_{gg}^{\text{NLO}} = \frac{\sigma^{\text{NLO}}(gg \rightarrow h \rightarrow 4\ell)}{\bar{\sigma}_{gg}^{\text{NLO}} \cdot \text{BR}(h \rightarrow 4\ell)}, \quad (8)$$

where we have displayed the NLO case for concreteness. The acceptances for the interference cross sections are obtained by subtraction in a similar way as the reference cross sections.

Some comments are in order regarding the branching ratio $\text{BR}(h \rightarrow 4\ell)$ in Eq. (8). First, MadGraph always computes the branching ratios at LO, even when cross sections are being generated at NLO. Therefore, for consistency we must divide out the LO branching ratio. Second, the branching ratio is defined as

$$\begin{aligned} \text{BR}(h \rightarrow 4\ell) &= \text{BR}(h \rightarrow ZZ^*) \\ &\times [\text{BR}(Z \rightarrow e^+e^-) + \text{BR}(Z \rightarrow \mu^+\mu^-)]^2, \end{aligned} \quad (9)$$

where $\text{BR}(Z \rightarrow e^+e^-) = \text{BR}(Z \rightarrow \mu^+\mu^-) = 3.43 \times 10^{-2}$ as computed by MadGraph. Here $\text{BR}(h \rightarrow ZZ^*)$ is to be computed according to Eqs. (5) and (6) using the same values of κ_g , $\bar{\kappa}_u$ and $\bar{\kappa}_d$ as were used in the generation of the decayed cross section. The relevant LO partial widths as computed by MadGraph are given in the first column of Table II.

The resulting detector acceptances for each of our reference cross sections are given in Table III. We give both LO and NLO acceptances for comparison. Note that the NLO acceptance for the gluon fusion process is about a third lower than that at LO, but the acceptances for the $u\bar{u}$ and $d\bar{d}$ fusion processes are quite similar at LO and NLO. At NLO, the acceptances for our reference cross sections are all roughly equal, $\epsilon_i^{\text{NLO}} \sim 0.2$ to within about 20%.

D. Signal strength constraint

We are now in a position to extract a relationship between κ_g , $\bar{\kappa}_u$ and $\bar{\kappa}_d$ which must be satisfied for the observed Higgs signal rate in the four-lepton final state to be the same as that in the SM. Our signal rate is given

	LO	NLO
ϵ_{gg}	0.306	0.204
$\epsilon_{u\bar{u}}$	0.184	0.196
$\epsilon_{d\bar{d}}$	0.229	0.237
$\epsilon_{u,\text{int}}$	—	0.186
$\epsilon_{d,\text{int}}$	—	0.207

TABLE III. Detector acceptances for each of the Higgs production processes in the 4ℓ final state.

	LO	NLO
α_u	-0.098	-0.197
α_d	-0.162	-0.250
β_u	—	0.387
β_d	—	0.315

TABLE IV. Coefficients for the signal rate constraint in Eq. (12), using LO or NLO cross sections and the Higgs decay widths from the LHC Higgs Cross Section Working Group [41].

by

$$\begin{aligned} R(pp \rightarrow h \rightarrow 4\ell) &= \left[\epsilon_{gg} \kappa_g^2 \bar{\sigma}_{gg} + \sum_{q=u,d} \epsilon_{q\bar{q}} \bar{\kappa}_q^2 \bar{\sigma}_{q\bar{q}} \right. \\ &\quad \left. + \sum_{q=u,d} \epsilon_{q,\text{int}} \kappa_g \bar{\kappa}_q \bar{\sigma}_{q,\text{int}} \right] \\ &\quad \times \frac{\Gamma_{ZZ^*}}{\kappa_g^2 \bar{\Gamma}_{gg} + \sum_{q=u,d} \bar{\kappa}_q^2 \bar{\Gamma}_{q\bar{q}} + \Gamma_{\text{else}}}. \end{aligned} \quad (10)$$

We set this equal to the SM signal rate,

$$R_{\text{SM}}(pp \rightarrow h \rightarrow 4\ell) = \frac{\epsilon_{gg} \bar{\sigma}_{gg} \Gamma_{ZZ^*}}{\bar{\Gamma}_{gg} + \Gamma_{\text{else}}}. \quad (11)$$

Rearranging this equality yields a quadratic equation for κ_g in terms of $\bar{\kappa}_u$ and $\bar{\kappa}_d$,

$$\kappa_g^2 + \alpha_u \bar{\kappa}_u^2 + \alpha_d \bar{\kappa}_d^2 + \beta_u \kappa_g \bar{\kappa}_u + \beta_d \kappa_g \bar{\kappa}_d = 1, \quad (12)$$

where the coefficients are given for $q = u, d$ by

$$\begin{aligned} \alpha_q &= \frac{\epsilon_{q\bar{q}} \bar{\sigma}_{q\bar{q}} (\bar{\Gamma}_{gg} + \Gamma_{\text{else}}) - \epsilon_{gg} \bar{\sigma}_{gg} \bar{\Gamma}_{q\bar{q}}}{\epsilon_{gg} \bar{\sigma}_{gg} \Gamma_{\text{else}}}, \\ \beta_q &= \frac{\epsilon_{q,\text{int}} \bar{\sigma}_{q,\text{int}} (\Gamma_{gg} + \Gamma_{\text{else}})}{\epsilon_{gg} \bar{\sigma}_{gg} \Gamma_{\text{else}}}. \end{aligned} \quad (13)$$

Note that Γ_{ZZ^*} has canceled out. Numerical results are given in Table IV.

As long as $\bar{\sigma}_{u,\text{int}}$ and $\bar{\sigma}_{d,\text{int}}$ are not too large, Eq. (12) defines an ellipsoid for the allowed values of the couplings. This in itself can be used to put constraints on $\bar{\kappa}_u$ and $\bar{\kappa}_d$ [29].

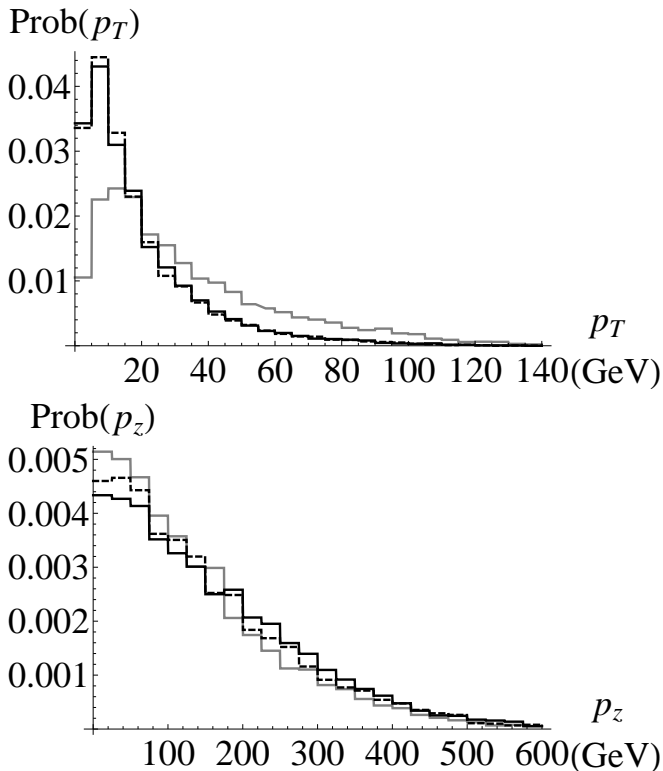


FIG. 3. Reconstructed Higgs p_T (top) and p_z (bottom) distributions for $gg \rightarrow h \rightarrow 4\ell$ (gray), $u\bar{u} \rightarrow h \rightarrow 4\ell$ (solid black), and $d\bar{d} \rightarrow h \rightarrow 4\ell$ (dashed black) after cuts, from 10,000 events generated at LO in QCD.

III. KINEMATIC DISCRIMINANTS

A. Asymmetry parameter

We now turn to the Higgs kinematic distributions. Figures 3 and 4 show the truth-level reconstructed Higgs p_T and p_z for $gg \rightarrow h \rightarrow 4\ell$, $u\bar{u} \rightarrow h \rightarrow 4\ell$, and $d\bar{d} \rightarrow h \rightarrow 4\ell$ at LO and NLO, respectively. To avoid clutter, we have not plotted the interference distributions at NLO, but we do take them into account below. At LO, the Higgs p_T is due entirely to the initial-state radiation as generated by Herwig++. The NLO calculation generates the momentum distribution of the first radiated parton at the matrix element level, so that we can expect a more accurate determination of the Higgs momentum distributions.

As is clear from Figs. 3 and 4, the Higgs p_T distribution in particular is rather different for the $gg \rightarrow h \rightarrow 4\ell$ process than for the $q\bar{q} \rightarrow h \rightarrow 4\ell$ processes. This will be the basis for the discriminating power of our method. One would also have expected the p_z distribution to be different for the gg fusion and $q\bar{q}$ fusion processes, given the very different momentum distributions carried by quarks and antiquarks in the proton. Unfortunately, the p_z distributions are made essentially identical by the lepton pseudorapidity cut, which removes the high- p_z tail for

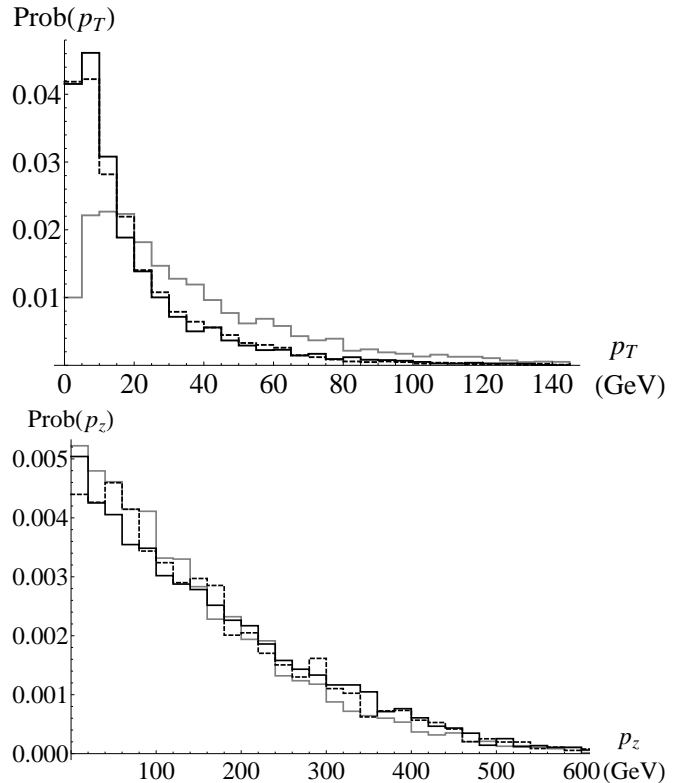


FIG. 4. The same as Fig. 3 but at NLO.

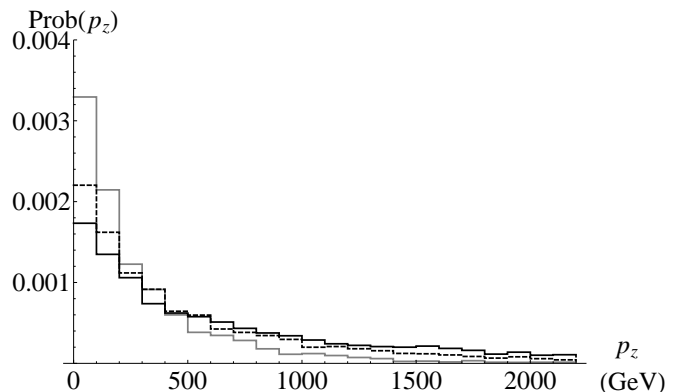


FIG. 5. Reconstructed Higgs p_z distributions at NLO, but omitting the lepton rapidity cut in Eq. (7). The lines are the same as in Fig. 4.

Higgs production from quark fusion. We illustrate this by showing in Fig. 5 the Higgs p_z distribution at NLO after applying only the lepton p_T and 4ℓ invariant mass cuts from Eq. (7). Indeed, we will find numerically that defining an asymmetry in a two-dimensional space of (p_T, p_z) does not increase our sensitivity over using only the p_T asymmetry. The p_z asymmetry may still be useful for the $h \rightarrow \gamma\gamma$ final state, in which only two objects have to fall within the pseudorapidity cut, or if the pseudorapidity coverage of the inner tracker is expanded in the course of the High-Luminosity LHC upgrades.

We define the asymmetry parameter for the reconstructed Higgs p_T distribution after cuts, for each of our production processes, as

$$A_j^T = \frac{N(p_{T,j} > p_T^{\text{cut}}) - N(p_{T,j} < p_T^{\text{cut}})}{N_{\text{tot}}}, \quad (14)$$

where $j = gg, u\bar{u}, d\bar{d}, u, \text{int}, \text{ or } d, \text{int}$. An analogous asymmetry can be defined for the p_z distributions. Here p_T^{cut} is some critical momentum value around which

the asymmetry parameter is calculated. The quantity $N(p_{T,j} > p_T^{\text{cut}})$ is the number of events of production mode j with p_T greater than p_T^{cut} , and $N_{\text{tot}} = N(p_{T,j} > p_T^{\text{cut}}) + N(p_{T,j} < p_T^{\text{cut}})$ is the total number of events.

The asymmetry parameter measured from LHC data will be a linear combination of the asymmetry parameters for the contributing production processes, weighted by the rate for that process. Since $\text{BR}(h \rightarrow 4\ell)$ is the same for each production process at fixed $\kappa_g, \bar{\kappa}_u$ and $\bar{\kappa}_d$, it cancels out of the definition in Eq. (14), and we can write

$$A_T = \frac{A_{gg}^T \kappa_g^2 \epsilon_{gg} \bar{\sigma}_{gg} + \sum_{q=u,d} A_{q\bar{q}}^T \bar{\kappa}_q^2 \epsilon_{q\bar{q}} \bar{\sigma}_{q\bar{q}} + \sum_{q=u,d} A_{q,\text{int}}^T \kappa_g \bar{\kappa}_q \epsilon_{q,\text{int}} \bar{\sigma}_{q,\text{int}}}{\kappa_g^2 \epsilon_{gg} \bar{\sigma}_{gg} + \sum_{q=u,d} \bar{\kappa}_q^2 \epsilon_{q\bar{q}} \bar{\sigma}_{q\bar{q}} + \sum_{q=u,d} \kappa_g \bar{\kappa}_q \epsilon_{q,\text{int}} \bar{\sigma}_{q,\text{int}}}. \quad (15)$$

An analogous expression holds for the p_z asymmetry parameter. We can eliminate κ_g from Eq. (15) by imposing the requirement that the total Higgs event rate in four leptons is consistent with the SM prediction, Eq. (12), thereby making our observable orthogonal to the total rate measurement. We can then write A_T as an analytic function of $\bar{\kappa}_u$ and $\bar{\kappa}_d$. A measurement of A_T then constrains these two parameters.

In order to implement this procedure, we must choose a value for p_T^{cut} and determine from Monte Carlo the asymmetry parameters A_{gg}^T , $A_{q\bar{q}}^T$, and $A_{q,\text{int}}^T$ (with $q = u, d$). Assuming that the measured asymmetry parameter is equal to the SM expectation, i.e., $A_T = A_{gg}^T$, we obtain the expected sensitivity to $\bar{\kappa}_u$ and $\bar{\kappa}_d$ as a function of the uncertainty on A_T .

At LO, the choice of p_T^{cut} is straightforward: we simply maximize the difference $\Delta A_q^T \equiv A_{gg}^T - A_{q\bar{q}}^T$ for $q = u, d$. Because the Higgs p_T distributions are so similar for the $u\bar{u}$ and $d\bar{d}$ fusion processes (Fig. 3), the optimum p_T^{cut} is the same within our Monte Carlo uncertainties for these two production processes. We find the optimum $p_T^{\text{cut}} = 18$ GeV for the LO distributions.

At NLO, the situation is more complicated due to the interference terms. Clearly we would like the resolving power to be as good as possible, which translates into the requirement that p_T^{cut} should be chosen to minimize the area of the constraint contour in the $(\bar{\kappa}_u, \bar{\kappa}_d)$ plane. To find this optimal cut we use the heuristic procedure of computing all the asymmetries on a grid of trial p_T^{cut} values, plotting the constraint contours for each cut, and selecting the smallest one. Using this procedure we find the optimum $p_T^{\text{cut}} = 20$ GeV for the NLO distributions. The fact that the optimal cut at NLO is so close to that found at LO gives us some confidence that the NLO corrections do not overwhelmingly change the picture. Using these cuts we compute the asymmetry parameters A_j^T for each production process; results are given in Table V.

	LO ($p_T^{\text{cut}} = 18$ GeV)	NLO ($p_T^{\text{cut}} = 20$ GeV)
A_{gg}^T	0.29 ± 0.01	0.27 ± 0.01
$A_{u\bar{u}}^T$	-0.24 ± 0.01	-0.35 ± 0.01
$A_{d\bar{d}}^T$	-0.26 ± 0.01	-0.32 ± 0.01
$A_{u,\text{int}}^T$	–	0.070 ± 0.001
$A_{d,\text{int}}^T$	–	-0.014 ± 0.001

TABLE V. Asymmetry parameters A_j^T for each production process calculated using optimized p_T^{cut} values at LO and NLO. The uncertainties represent the Monte Carlo statistical uncertainties.

B. Sensitivity estimate

In what follows we assume that the experimental measurement of A_T will be consistent with the SM expectation (i.e., $A_T = A_{gg}^T$) and proceed to estimate the constraint that can be placed upon $\bar{\kappa}_u$ and $\bar{\kappa}_d$ at the 95% confidence level.

The statistical uncertainty on A_T is given by

$$\sigma_{A_T}^{\text{stat}} = \sqrt{\frac{1 - A_T^2}{N_{\text{tot}}}}; \quad (16)$$

see Appendix A for a derivation. Assuming SM production and decay, the total number of events in the four-lepton decay channel is given by

$$N_{\text{tot}} = \epsilon_{gg} \bar{\sigma}_{gg} \text{BR}(h \rightarrow 4\ell) \int \mathcal{L} dt, \quad (17)$$

where $\int \mathcal{L} dt$ is the integrated luminosity and $\text{BR}(h \rightarrow 4\ell) = 1.26 \times 10^{-4}$ from Ref. [41]. We give the expected number of 4ℓ events and the corresponding statistical uncertainty on the asymmetry parameter for various integrated luminosities in Table VI.

Combining Eqs. (15) and (12), plugging in numbers, and setting the asymmetry parameter equal to its SM

$\int \mathcal{L} dt$	N_{tot} (LO)	$\sigma_{A_T}^{\text{stat}}$ (LO)	N_{tot} (NLO)	$\sigma_{A_T}^{\text{stat}}$ (NLO)
30 fb $^{-1}$	20	0.22	30	0.18
300 fb $^{-1}$	200	0.071	300	0.056
3000 fb $^{-1}$	2000	0.022	3000	0.018

TABLE VI. Expected number of 4ℓ signal events for gluon-fusion Higgs production with decays to four leptons at the 13 TeV LHC, assuming SM production and decay rates, and the corresponding statistical uncertainty on the asymmetry parameter A_T .

expectation within uncertainties, at LO we have

$$A_T^{\text{LO}} = \frac{0.29 - 0.089\bar{\kappa}_u^2 - 0.064\bar{\kappa}_d^2}{1.0 + 0.59(\bar{\kappa}_u^2 + \bar{\kappa}_d^2)} = 0.29 \pm 2\sigma_{A_T}^{\text{stat}}. \quad (18)$$

This expression defines a circle in the $(\bar{\kappa}_u, \bar{\kappa}_d)$ plane with radius determined by $\sigma_{A_T}^{\text{stat}}$. This is shown for 300 and 3000 fb $^{-1}$ in Fig. 6 (dashed lines).

At NLO, the functional form is more complicated; we have

$$\kappa_g = -0.19\bar{\kappa}_u - 0.16\bar{\kappa}_d \pm \sqrt{1.0 + 0.23\bar{\kappa}_u^2 + 0.27\bar{\kappa}_d^2 + 0.061\bar{\kappa}_u\bar{\kappa}_d}, \quad (19)$$

$$A_T^{\text{NLO}} = \frac{0.27\kappa_g^2 - 0.14\bar{\kappa}_u^2 - 0.11\bar{\kappa}_d^2 + 0.025\bar{\kappa}_u\kappa_g - 0.0040\bar{\kappa}_d\kappa_g}{1.0\kappa_g^2 + 0.40\bar{\kappa}_u^2 + 0.35\bar{\kappa}_d^2 + 0.35\bar{\kappa}_u\kappa_g + 0.29\bar{\kappa}_d\kappa_g}. \quad (20)$$

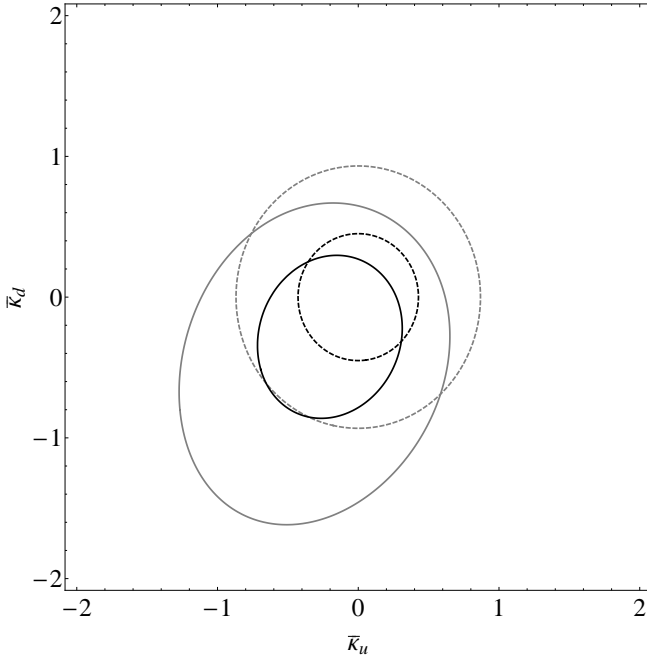


FIG. 6. Projected 95% confidence level constraints on $\bar{\kappa}_u$ and $\bar{\kappa}_d$ from the Higgs p_T asymmetry parameter in the four-lepton final state at LO (dashed) and NLO (solid), with 300 fb $^{-1}$ (larger gray contours) and 3000 fb $^{-1}$ (smaller black contours) at the 13 TeV LHC. Uncertainties are statistical only.

We will choose the plus sign in the expression for κ_g , so that κ_g is positive (choosing the minus sign is equivalent to replacing $(\bar{\kappa}_u, \bar{\kappa}_d) \rightarrow (-\bar{\kappa}_u, -\bar{\kappa}_d)$ in Fig. 6). The terms in A_T^{NLO} in which $\bar{\kappa}_u$ and $\bar{\kappa}_d$ enter linearly introduce an asymmetry in the constraint that depends on the signs of $\bar{\kappa}_u$ and $\bar{\kappa}_d$. Setting $A_T^{\text{NLO}} = 0.27 \pm 2\sigma_{A_T}^{\text{stat}}$ yields the constraint contours shown by solid lines in Fig. 6 for 300 and 3000 fb $^{-1}$. These constraints are given numerically in Table VII.

	300 fb $^{-1}$	3000 fb $^{-1}$
$\bar{\kappa}_u$	(-1.3, 0.67)	(-0.73, 0.33)
$\bar{\kappa}_d$	(-1.6, 0.69)	(-0.88, 0.32)

TABLE VII. Projected 95% confidence level constraints on $\bar{\kappa}_u$ and $\bar{\kappa}_d$ from the Higgs p_T asymmetry parameter in the four-lepton final state at NLO, with 300 and 3000 fb $^{-1}$ at the 13 TeV LHC. Uncertainties are statistical only.

IV. DISCUSSION AND CONCLUSIONS

To get a sense of how reasonable our results are, we calculate the individual components of the Higgs cross section and decay width for our tightest limits at 3000 fb $^{-1}$. We consider (1) $\bar{\kappa}_u = 0.33$, $\bar{\kappa}_d = 0$, for which Eq. (12) yields $\kappa_g = 0.949$, and (2) $\bar{\kappa}_d = 0.32$, $\bar{\kappa}_u = 0$, for which Eq. (12) yields $\kappa_g = 0.963$.

We first consider the Higgs production cross section. At NLO we compute the SM Higgs production cross section from gluon fusion, $\bar{\sigma}_{gg} = 37.3$ pb. For $\bar{\kappa}_u = 0.33$, $\bar{\kappa}_d = 0$, and $\kappa_g = 0.949$, we find $\sigma_{gg} = 33.6$ pb, $\sigma_{u\bar{u}} = 1.68$ pb, and $\sigma_{u,\text{int}} = 4.54$ pb, for a total cross section (before cuts) of 39.8 pb. Thus at this parameter point the $u\bar{u}$ production process constitutes about 4% of the total rate and the interference term constitutes a further 11%.

For $\bar{\kappa}_d = 0.32$, $\bar{\kappa}_u = 0$, and $\kappa_g = 0.963$, we find $\sigma_{gg} = 34.6$ pb, $\sigma_{d\bar{d}} = 1.15$ pb, and $\sigma_{d,\text{int}} = 3.27$ pb, for a total cross section (before cuts) of 39.0 pb. Thus at this parameter point the $d\bar{d}$ production process constitutes about 3% of the total rate and the interference term constitutes a further 8%. The greater sensitivity in the $\bar{\kappa}_d \neq 0$ case can be explained by the greater difference between A_{gg}^T and $A_{d,\text{int}}^T$ compared to the difference between A_{gg}^T and $A_{u,\text{int}}^T$ (see Table V).

The Higgs branching ratios are also affected. In the SM

we have $\text{BR}(h \rightarrow gg) = 8.6\%$ [41]. For $\bar{\kappa}_u = 0.33$, $\bar{\kappa}_d = 0$, and $\kappa_g = 0.949$, this becomes $\text{BR}(h \rightarrow gg) = 7.3\%$ and $\text{BR}(h \rightarrow u\bar{u}) = 6.0\%$. Similarly, for $\bar{\kappa}_d = 0.32$, $\bar{\kappa}_u = 0$, and $\kappa_g = 0.963$, we obtain $\text{BR}(h \rightarrow gg) = 7.6\%$ and $\text{BR}(h \rightarrow d\bar{d}) = 5.6\%$. If techniques to separate gluon jets from quark jets [26] become sufficiently advanced, light quark branching fractions at this level may be able to be probed at a future International Linear e^+e^- Collider. For comparison, the SM decay branching ratio for $h \rightarrow c\bar{c}$ is 2.9% [41] and for $h \rightarrow s\bar{s}$ is below 10^{-3} .

Throughout this analysis we have ignored the effect of experimental and theoretical systematic uncertainties. These are beyond the scope of this proof-of-concept, but may be of great concern, especially the theoretical uncertainties on the Higgs p_T distributions in the various production channels studied. We note that with 3000 fb^{-1} , the statistical uncertainty on the asymmetry in the 4ℓ channel is 7% ; this sets the scale for whether systematic uncertainties will have a significant effect on our results.

To summarize, we have presented a method for constraining the up and down quark Yukawa couplings at a level comparable to competing approaches using Higgs p_T distributions in the four-lepton final state. Our method is orthogonal to the constraint from a global fit to Higgs signal strengths in various production and decay channels, and hence can be combined to further increase the precision. We find that 3000 fb^{-1} of integrated luminosity at the 13 TeV LHC can constrain $\bar{\kappa}_u \lesssim 0.33$ and $\bar{\kappa}_d \lesssim 0.32$. The constraints are weaker for negative $\bar{\kappa}_u$ and $\bar{\kappa}_d$ due to interference effects. Including the two-photon final state may improve the sensitivity.

Note added: While we were finalizing the manuscript, we became aware of two recent papers [42, 43] that also use Higgs p_T distributions to constrain the Higgs couplings to quarks. Ref. [42] considers constraints on the bottom, charm, and strange Yukawa couplings, while Ref. [43] addresses the up and down quark Yukawa couplings. Ref. [43] fits the Higgs p_T distribution to published LHC results combining the four-lepton and two-photon final states, and extrapolates the expected sensi-

tivity to 300 fb^{-1} at 13 TeV, and find constraints on $\bar{\kappa}_{u,d}$ roughly comparable to ours at this luminosity.

ACKNOWLEDGMENTS

This work was supported by the Natural Sciences and Engineering Research Council of Canada. We thank Andrea Peterson for help with MadGraph and for providing a modified version of the NLO Higgs Characterization model file with Higgs couplings to up and down quarks.

Appendix A: Statistical uncertainty on the asymmetry

Each event that we see has a definite p_T of the Higgs boson, but depending on whether or not a given value is less than p_T^{cut} it either contributes 1 or 0 to the quantity $N(p_T < p_T^{\text{cut}})$. Hence, we can interpret $N(p_T < p_T^{\text{cut}})/N_{\text{tot}}$ as the sample mean of a set of N_{tot} Bernoulli trials with probability of success $\mathcal{P} = \int_0^{p_T^{\text{cut}}} f_T(x) dx$ where $f_T(x)$ is the underlying physical distribution of p_T . The expected value of the sample mean is the mean of the underlying Bernoulli distribution, \mathcal{P} . The variance of the sample mean is the variance of the underlying Bernoulli distribution, $\mathcal{P}(1 - \mathcal{P})$, divided by the number of samples. Therefore, the expected value and variance of A_T are

$$E[A_T] = 1 - 2\mathcal{P} = A_T, \quad (\text{A1})$$

$$V[A_T] = \frac{4}{N_{\text{tot}}} \mathcal{P}(1 - \mathcal{P}) = \frac{1}{N_{\text{tot}}} (1 - A_T^2). \quad (\text{A2})$$

Hence, given a measurement of A_T , the statistical uncertainty on A_T is

$$\sigma_{A_T}^{\text{stat}} = \sqrt{\frac{1 - A_T^2}{N_{\text{tot}}}}. \quad (\text{A3})$$

Why is the statistical uncertainty zero when $A_T = \pm 1$? In these cases, p_T^{cut} is either at exactly zero or infinity. Hence, no matter what the distributions are doing, A_T will be identically equal to ± 1 .

-
- [1] G. Aad *et al.* [ATLAS Collaboration], “Observation of a new particle in the search for the Standard Model Higgs boson with the ATLAS detector at the LHC,” *Phys. Lett. B* **716**, 1 (2012) [arXiv:1207.7214 [hep-ex]].
 - [2] S. Chatrchyan *et al.* [CMS Collaboration], “Observation of a new boson at a mass of 125 GeV with the CMS experiment at the LHC,” *Phys. Lett. B* **716**, 30 (2012) [arXiv:1207.7235 [hep-ex]].
 - [3] V. Khachatryan *et al.* [CMS Collaboration], “Precise determination of the mass of the Higgs boson and tests of compatibility of its couplings with the standard model predictions using proton collisions at 7 and 8 TeV,” *Eur. Phys. J. C* **75**, no. 5, 212 (2015) [arXiv:1412.8662 [hep-ex]].
 - [4] G. Aad *et al.* [ATLAS Collaboration], “Measurements of the Higgs boson production and decay rates and coupling strengths using pp collision data at $\sqrt{s} = 7$ and 8 TeV in the ATLAS experiment,” *Eur. Phys. J. C* **76**, no. 1, 6 (2016) [arXiv:1507.04548 [hep-ex]].
 - [5] G. Aad *et al.* [ATLAS Collaboration], “Search for the Standard Model Higgs boson produced in association with top quarks and decaying into $b\bar{b}$ in pp collisions at $\sqrt{s} = 8$ TeV with the ATLAS detector,” *Eur. Phys. J. C* **75**, no. 7, 349 (2015) [arXiv:1503.05066 [hep-ex]].
 - [6] G. Aad *et al.* [ATLAS Collaboration], “Search for $H \rightarrow \gamma\gamma$ produced in association with top quarks and con-

- straints on the Yukawa coupling between the top quark and the Higgs boson using data taken at 7 TeV and 8 TeV with the ATLAS detector,” *Phys. Lett. B* **740**, 222 (2015) [arXiv:1409.3122 [hep-ex]].
- [7] G. Aad *et al.* [ATLAS Collaboration], “Search for the $b\bar{b}$ decay of the Standard Model Higgs boson in associated $(W/Z)H$ production with the ATLAS detector,” *JHEP* **1501**, 069 (2015) [arXiv:1409.6212 [hep-ex]].
- [8] V. Khachatryan *et al.* [CMS Collaboration], “Search for a Standard Model Higgs Boson Produced in Association with a Top-Quark Pair and Decaying to Bottom Quarks Using a Matrix Element Method,” *Eur. Phys. J. C* **75**, no. 6, 251 (2015) [arXiv:1502.02485 [hep-ex]].
- [9] V. Khachatryan *et al.* [CMS Collaboration], “Search for the associated production of the Higgs boson with a top-quark pair,” *JHEP* **1409**, 087 (2014) [Erratum: *JHEP* **1410**, 106 (2014)] [arXiv:1408.1682 [hep-ex]].
- [10] S. Chatrchyan *et al.* [CMS Collaboration], “Search for the standard model Higgs boson produced in association with a W or a Z boson and decaying to bottom quarks,” *Phys. Rev. D* **89**, no. 1, 012003 (2014) [arXiv:1310.3687 [hep-ex]].
- [11] CMS Collaboration, “Search for H to $b\bar{b}$ in association with single top quarks as a test of Higgs couplings,” CMS-PAS-HIG-14-015.
- [12] S. Chatrchyan *et al.* [CMS Collaboration], “Evidence for the direct decay of the 125 GeV Higgs boson to fermions,” *Nature Phys.* **10**, 557 (2014) [arXiv:1401.6527 [hep-ex]].
- [13] G. F. Giudice and O. Lebedev, “Higgs-dependent Yukawa couplings,” *Phys. Lett. B* **665**, 79 (2008) [arXiv:0804.1753 [hep-ph]].
- [14] F. J. Botella, G. C. Branco, M. N. Rebelo and J. I. Silva-Marcos, “What if the Masses of the First Two Quark Families are not Generated by the Standard Higgs?,” arXiv:1602.08011 [hep-ph].
- [15] R. Harnik, J. Kopp and J. Zupan, “Flavor Violating Higgs Decays,” *JHEP* **1303**, 026 (2013) [arXiv:1209.1397 [hep-ph]].
- [16] M. Bauer, M. Carena and K. Gemmler, “Creating the Fermion Mass Hierarchies with Multiple Higgs Bosons,” arXiv:1512.03458 [hep-ph].
- [17] D. Ghosh, R. S. Gupta and G. Perez, “Is the Higgs Mechanism of Fermion Mass Generation a Fact? A Yukawa-less First-Two-Generation Model,” *Phys. Lett. B* **755**, 504 (2016) [arXiv:1508.01501 [hep-ph]].
- [18] Y. Meng, Z. Surujon, A. Rajaraman and T. M. P. Tait, “Strange Couplings to the Higgs,” *JHEP* **1302**, 138 (2013) [arXiv:1210.3373 [hep-ph]].
- [19] C. Delaunay, T. Golling, G. Perez and Y. Soreq, “Enhanced Higgs boson coupling to charm pairs,” *Phys. Rev. D* **89**, no. 3, 033014 (2014) [arXiv:1310.7029 [hep-ph]].
- [20] G. Perez, Y. Soreq, E. Stamou and K. Tobioka, “Constraining the charm Yukawa and Higgs-quark coupling universality,” *Phys. Rev. D* **92**, no. 3, 033016 (2015) [arXiv:1503.00290 [hep-ph]].
- [21] G. Perez, Y. Soreq, E. Stamou and K. Tobioka, “Prospects for measuring the Higgs boson coupling to light quarks,” *Phys. Rev. D* **93**, no. 1, 013001 (2016) [arXiv:1505.06689 [hep-ph]].
- [22] G. T. Bodwin, F. Petriello, S. Stoynev and M. Velasco, “Higgs boson decays to quarkonia and the $H\bar{c}c$ coupling,” *Phys. Rev. D* **88**, no. 5, 053003 (2013) [arXiv:1306.5770 [hep-ph]].
- [23] A. L. Kagan, G. Perez, F. Petriello, Y. Soreq, S. Stoynev and J. Zupan, “Exclusive Window onto Higgs Yukawa Couplings,” *Phys. Rev. Lett.* **114**, no. 10, 101802 (2015) [arXiv:1406.1722 [hep-ph]].
- [24] M. Knig and M. Neubert, “Exclusive Radiative Higgs Decays as Probes of Light-Quark Yukawa Couplings,” *JHEP* **1508**, 012 (2015) [arXiv:1505.03870 [hep-ph]].
- [25] H. Baer *et al.*, “The International Linear Collider Technical Design Report - Volume 2: Physics,” arXiv:1306.6352 [hep-ph].
- [26] V. Rentala, N. Vignaroli, H. n. Li, Z. Li and C.-P. Yuan, “Discriminating Higgs production mechanisms using jet energy profiles,” *Phys. Rev. D* **88**, no. 7, 073007 (2013) [arXiv:1306.0899 [hep-ph]].
- [27] K. A. Olive *et al.* [Particle Data Group Collaboration], “Review of Particle Physics,” *Chin. Phys. C* **38**, 090001 (2014).
- [28] A. David *et al.* [LHC Higgs Cross Section Working Group Collaboration], “LHC HXSWG interim recommendations to explore the coupling structure of a Higgs-like particle,” arXiv:1209.0040 [hep-ph].
- [29] Y. Zhou, “Constraining the Higgs boson coupling to light quarks in the $H\rightarrow ZZ$ final states,” *Phys. Rev. D* **93**, no. 1, 013019 (2016) [arXiv:1505.06369 [hep-ph]].
- [30] C. Delaunay, R. Ozeri, G. Perez and Y. Soreq, “Probing The Atomic Higgs Force,” arXiv:1601.05087 [hep-ph].
- [31] F. Bishara, J. Brod, P. Uttayarat and J. Zupan, “Non-standard Yukawa Couplings and Higgs Portal Dark Matter,” *JHEP* **1601**, 010 (2016) [arXiv:1504.04022 [hep-ph]].
- [32] J. Alwall *et al.*, “The automated computation of tree-level and next-to-leading order differential cross sections, and their matching to parton shower simulations,” *JHEP* **1407**, 079 (2014) [arXiv:1405.0301 [hep-ph]].
- [33] S. Chatrchyan *et al.* [CMS Collaboration], “Measurement of the properties of a Higgs boson in the four-lepton final state,” *Phys. Rev. D* **89**, no. 9, 092007 (2014) [arXiv:1312.5353 [hep-ex]].
- [34] F. Maltoni, K. Mawatari and M. Zaro, “Higgs characterisation via vector-boson fusion and associated production: NLO and parton-shower effects,” *Eur. Phys. J. C* **74**, no. 1, 2710 (2014) [arXiv:1311.1829 [hep-ph]].
- [35] F. Demartin, F. Maltoni, K. Mawatari, B. Page and M. Zaro, “Higgs characterisation at NLO in QCD: CP properties of the top-quark Yukawa interaction,” *Eur. Phys. J. C* **74**, no. 9, 3065 (2014) [arXiv:1407.5089 [hep-ph]].
- [36] F. Demartin, F. Maltoni, K. Mawatari and M. Zaro, “Higgs production in association with a single top quark at the LHC,” *Eur. Phys. J. C* **75**, no. 6, 267 (2015) [arXiv:1504.00611 [hep-ph]].
- [37] F. Demartin, E. Vryonidou, K. Mawatari and M. Zaro, “Higgs characterisation: NLO and parton-shower effects,” arXiv:1505.07081 [hep-ph].
- [38] R. D. Ball *et al.* [NNPDF Collaboration], “Parton distributions with QED corrections,” *Nucl. Phys. B* **877**, 290 (2013) [arXiv:1308.0598 [hep-ph]].
- [39] M. Bahr *et al.*, “Herwig++ Physics and Manual,” *Eur. Phys. J. C* **58**, 639 (2008) [arXiv:0803.0883 [hep-ph]].
- [40] M. Cacciari, G. P. Salam and G. Soyez, “FastJet User Manual,” *Eur. Phys. J. C* **72**, 1896 (2012) [arXiv:1111.6097 [hep-ph]].
- [41] S. Heinemeyer *et al.* [LHC Higgs Cross Section Working Group Collaboration], “Handbook of LHC Higgs Cross

- Sections: 3. Higgs Properties,” arXiv:1307.1347 [hep-ph].
- [42] F. Bishara, U. Haisch, P. F. Monni and E. Re, “Constraining Light-Quark Yukawa Couplings from Higgs Distributions,” arXiv:1606.09253 [hep-ph].
- [43] Y. Soreq, H. X. Zhu and J. Zupan, “Light quark Yukawa couplings from Higgs kinematics,” arXiv:1606.09621 [hep-ph].